Silver(Ag) Improvements on The Structural, Creep Resistance and Electrical Conductivity Properties of Eutectic Sn-9Zn Alloys

M.S.N. Al-Salmi[(1),] Gobran N. Ali [(2)], A.M. Aljarbani [(2)] , Shakib. Alsowidy[*(2),] and Abdullah T. Naji[(3)]
[(1)] Physics Department, Faculty of Applied Science, Thamar University, Yemen,
[(2)] Physics Department, Faculty of Science, Sana'a University, Yemen.
[(3)] Biomedical Engineering Department, Faculty of Engineering, University of Science and Technology, Yemen.
Correspondent Author: *Mohammedalsalmi99@gmail.com*
DOI: https://doi.org/10.56807/buj.v2i3.116

Abstract

The structural, creep resistance and electrical Conductivity properties of Sn-9Zn alloys with Ag-addition in concentrations (0.1 and 0.3 % Wt.) have been investigated using x-ray diffractions (XRD), Creep testing machine and DC circuit respectively. The three samples were prepared from high purity 99.99% by melting technique in the Pyrex tubs with $CaCl_2$ to invade the oxidation. Patterns of XRD showed thst the Sn–9Zn alloy was primarily composed of two phases; a body centered tetragonal β-Sn matrix phase, and a secondary phase of hexagonal Zn. While with adding Ag (0.1 and 0.3 % Wt.) to Sn-9Zn alloy the results showed new peaks in the ternary compositions, such as β-Sn, Zn, Ag3Sn and AgZn3 phases respectively. The average of particle size (D) of β-Sn matrix was decreased with increasing Ag-adding, whereas the dislocation density (δ) increased with increasing addition. Creep properties of Sn-9Zn and Sn–9Zn–xAg alloys were examined at different temperature (25, 40, and 80 ℃) under two constant loads (18.7 MPa and 24.9 MPa). The creep behaviors of ternary alloys were higher than the Sn-9Zn alloy with all different temperatures and two constant loads, due to the refinement structure and formation of new IMCs. Values of stress exponents (n) were found to be in the range of 2.51 to 6.68 for all alloys. Values of activation energy (Q) of alloys were found to be in the range of 36.48 to 41.14 kJ/mol for $\sigma = 18.7$ Mpa and 27 to 34.3 kJ/mol for $\sigma = 24.94$ Mpa. The electrical conductivity of samples was calculated at room temperature (25℃), its values increased with Ag-additions.

Keywords: *Sn-9Zn Lead-Free Alloy; Phases; Ag-Additions; Creep Resistance Properties; Electrical conductivity*

تحسينات الفضة على الخواص التركيبية ومقاومة الزحف والموصلية الكهربائية لسبائك (قصدير- 9خارصين) المنصهرة

الملخص

قيست الخواص التركيبية ومقاومة الزحف والموصلية الكهربائية لسبائك (قصدير-9خارصين) مع اضافه الفضة بتراكيز (0.1 & 0.3 wt.%) باستخدام جهاز حيود الأشعة السينية وجهاز اختبار الزحف الميكانيكي ودائرة التيار المستمر، على التوالي. تم تحضير الثلاث العينات بنقاوة عالية (99.99%) باستخدام تقنية الصهر في انابيب بيركس مع إضافة كلوريد الكالسيوم لمنع التأكسد. أظهرت تحاليل جهاز حيود الأشعة السينية للسبيكة الثنائية (قصدير-9خارصين) انها مركب ابتدائي من طورين، الأول طور رباعي متمركز الجسم β-Sn والثاني طور خارصين سداسي، بينما مع إضافة الفضة للسبيكة الثنائية أظهرت أنماط حيود الأشعة السينية قمم جديدة في المركبات الثلاثية مثل β-Sn, Zn, (Ag3Sn & AgZn3). متوسط الحجم الحبيبي للطور (β-Sn) يتناقص مع زيادة إضافة الفضة بينما كثافة الانخلاع تتزايد مع زيادة إضافة الفضة. خصائص الزحف دُرست للثلاث العينات عند درجات حرارة مختلفة (25 ,40 و80 درجة مئوية) تحت تأثير حملين (18.7 و24.9 ميجا باسكال). أظهرت نتائج سلوك الزحف لسبائك ان السبائك الثلاثية لها مقاومة زحف اعلى من السبيكة الثنائية، بسبب تعزيز التركيب وظهور مركبات بينية في السبائك. تم الحصول على قيم أس الاجهاد في نطاق 2.51 الى 6.68 لجميع السبائك. تم الحصول على قيم طاقة التنشيط للسبائك في حدود 36.48 الى 41.14 كيلو جول/مول للحمل 18.7 ميجا باسكال و27 الى 34.3 كيلو جول / مول للحمل 24.94 ميجا باسكال. الموصلية الكهربائية قيست عند درجة حرارة الغرفة (25 درجة مئوية)، قيمها تزايدت مع زيادة إضافة تركيز الفضة.

1. Introduction

Alloys solders (Sn–Pb) have been widely used in the field of electronic packaging because of its excellent characteristics, such as low melting point (183 °C), strong mechanical properties, low cost and low price (Peng et al., 2019, Zhang and Tu, 2014). Sn-Pb alloy welders, however are toxic. With the growing recognition of environmental protection and the issuance of the 'lead restriction order' by several countries, the use of Pb has been significantly reduced (Vuong et al., 2018, Zhu et al., 2019, Peng et al., 2019) . New forms of lead-free alloys, such as: Sn-10Sb (271℃), Sn-58Bi (138℃) Sn-9Zn (198℃), Sn-3.5Ag (221℃), Sn-0.7Cu (227℃), and Sn-Ag-Cu (217℃), have recently been investigated by many researchers for green electronic devices (Kotadia et al., 2014, Gain and Zhang, 2016, Cheng et al., 2017, Ahmed et al., 2010). Due to its special low temperature characteristics, the low temperature solder (In-based, Sn-Bi, Sn-Zn) has great advantages in aerospace and through-hole technology assemblies in IBM mainframe (Xu et al., 2020). The cost-effective and better mechanical properties of the eutectic Sn-9Zn material, with a low melting temperature close to that of the conventional Sn-37Pb alloy (183℃), have caused it to be considered one of the best choices for applications in green electronic products among the above-mentioned Sn-based alloys. However, to extend its applications in modern green electronics (Knott and Mikula, 2002, Xu et al., 2020), its low oxidation resistance and micro-void formation need to be resolved. The addition of an effective secondary step for the creation of Zn-based IMCs (Garcia et al., 2010, Liu et al., 2014) is the eutectic Sn-9Zn alloy. At the same time, Chen et al. (Chen et al., 2009) studied the (0, 0.1, 0.3, 0.5, 1wt. percent) Ag-addition reinforcements on the microstructure and mechanical performance behavior of the Sn-9Zn solder alloy. It was found that the composite soldiers and their joints displayed improved mechanical properties, as well as AgZn3 intermetallic compounds in the Sn-9Zn solder alloy. Guoda *et al*, (Guoda et al., 2014) Studied the structure properties of Sn-9Zn-1Ag solder alloy, three-phase mixture was calculated in the structure properties of the alloy; tetragonal Sn as a solid solution, Zn phase, and intermetallic compound Ag-Zn. Influence of Cu Addition on the transient creep characteristics of Sn-9Zn-1.5Ag Solder Alloy studied by (Salem, 2020), XRD assessed, during solidification, the two samples provided additional contained phases of the intermetallic compound IMCs, Cu5Zn8, Ag3Sn, and AgZn3. Shrestha *et al*. (Shrestha et al., 2014) studied the creep properties of Sn-xZn solders (x=9, 20, 25 wt. percent) and found that the solders exhibited approximately (n= 5.0) exponents of stress. In the temperature range between 298 and 398 K and under constant strain rates, Hamada *et al*. (Hamada et al., 2010) analyzed the creep activity of Sn and Sn-xZn (x= 0.1 wt. percent and 0.4 wt. percent). They concluded that the addition of Zn Increases Sn's creep resistance, and found the value of the stress exponent to be equal to (n= 7), indicating that a dislocation pipe diffusion is the control mechanism. The effect of Ni and Sb additions on the microstructure, thermal and mechanical properties of Sn-9 wt. percent Zn was investigated by El-Daly et al. (El-Daly et al., 2014) The values of the stress exponent and activation energies were compatible with those cited for dislocation

climbing, they pointed out. In order to improve the microstructure and mechanical properties, the composite approach has been developed, where the Ag Nano sized particles act as pinning centers for the dislocation movements. The effect of an Ag nanoparticle addition to the Sn-9Zn alloy was investigated by Gain, *et.al*, (Gain and Zhang, 2020) and the appearance of IMCs AgZn3 in the Sn-9Zn-0.5Ag nanoparticle solder alloy was identified. The mechanical output reinforcements also include the Nano Sized Ag. An attempt is made in the present work to show the effect of 0.1 and 0.3 wt. percent Ag-addition on the structural, creep resistance and electrical conductivity properties of alloys (Sn-9 wt. %Zn- x wt. %Ag).

2. *Experimental procedures*

2.1. Materials preparation

Sn – 9wt.% Zn, Sn-9Zn-0.3wt.% Ag and Sn – 9wt.%Zn -0.1wt.% Ag alloys were prepared. The purity of Sn, Zn and Ag elements are about 99.99%. Every sample was put inside the Pyrex tub with $CaCL_2$ (to invaded the oxidation the compositions), and they have been melted at approximately 200 °C above their melting points by an electric furnace at (T= 750 ˚C $\pm$ 5 ˚C, around 3 hrs.) with shaking to achieve homogenization. To obtain samples fully precipitated phases, samples were left inside the furnace to solidify slowly to room temperature. The samples were polished using grades of silicon paper and then washed in a solution of (CH_3COCH_3). After that, the samples were drawn into two groups by using the rolling mechanism technique; the first group was as wires of a diameter (D= 1 mm) and a length (L= 80 mm) for the creep properties testing. The second group was as small sheets for structural investigations (XRD). The samples were polished using grades of silicon paper and then washed in a solution of (CH_3COCH_3). In order to remove residual stress and defects, the samples were annealed at (T= 100 ˚C ± 2 ˚C) for 6 hours and left to cool slowly to room temperature with cooling rate of 1˚C / min, and polished again.

2.2. Materials investigation

X-ray Shimadzu DX-720 model with CuKα radiation (λ=1.54056 Å) was used for XRD analysis. The XRD curves of the samples were constructed in the 2θ range of 5–75°. The operating source was under an accelerating voltage of 40 kV and a tube current of 20 mA, with a constant scanning rate of 0.02/1sec. The tensile creep tests were implemented on all samples at different temperatures (25, 40, and 80˚C) under constant loads (18.7 and 24.94) MPa using a computerized vertical tensile technique. Electrical resistivity and conductivity are measured using a simple circuit (DC) of Ohm's law.

3. Results and discussion

The findings of this study are classified to structural, Mechanical and electrical properties of Sn-9Zn alloys with Ag-addition in concentrations (0.1 and 0.3 % Wt.) as follows:

3.1. Structural analysis

According to investigated materials structural, figure 1 (a, b and c) showed the x-ray diffraction (XRD) curves for Sn-9Zn and Sn–9Zn–x Ag solders with (x = 0, 0.1, and 0.3 wt.%) respectively.

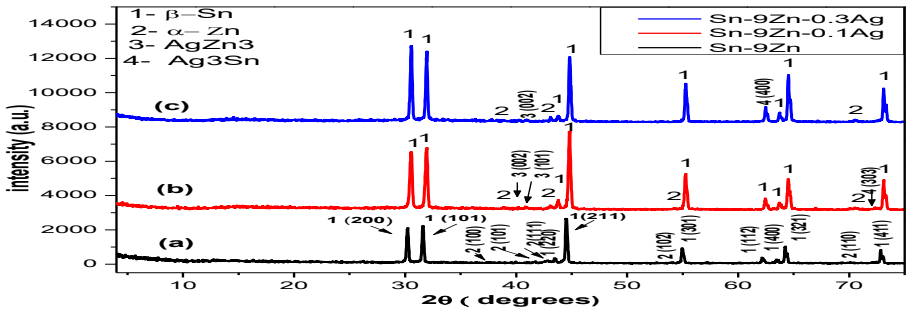

Fig. (1): XRD patterns for all three samples; **(a)** Sn-9Zn, **(b)** Sn-9Zn-0.1Ag and **(c)** Sn-9Zn-0.3Ag.

The obtained diffraction patterns have been compared with standard powder diffraction data (pdf) using search / match process of measured data with appropriate reference file using jade6.5 software. Figure (1a) showed the XRD results of Sn-9Zn alloy, which show: (i) large peaks intensity of Body cantered tetragonal β-Sn-rich phase, (ii) small peaks of Hexagonal Zn phases through the entire Alloy. The structure of 0.1 and 0.3Ag-containing Alloys showed additional IMCs of Orthorhombic Ag3Sn and Hexagonal AgZn3, respectively, while dispersed in β-Sn rich matrix and Zn Phases Fig. 1(b and c). The phases with **(**JCPDS-ICDD) Reverence card no. PDF#04-0673, PDF#04-0831, PDF#44-1300 and PDF#25-1325 for Sn, Zn, Ag3Sn and AgZn3 respectively are marked in Figure 1(a, b and c). Also the peaks of the eutectic α-Zn phase decreased in the Ag-containing alloys, as documented by (Salem, 2020, Guoda et al., 2014). So, the formation of Ag–Zn compounds reduced the Zn content in the alloy matrix and enhances the formation of the hypoeutectic structure in the Sn–9Zn–0.1Ag and Sn–9Zn–0.3Ag solder alloys (El-Daly et al., 2015). The particle sizes and dislocation density were studied as function of Ag- addition as showed in Fig. (2). The particle size for β-Sn, Ag_3Sn and AgZn3 in all the Sn–9Zn–x Ag alloys were calculated according to Scherer Formula (Williamson and Hall, 1953): $D = \frac{0.9\lambda}{\beta \cos\theta}$ ---- (1), where: β is the broadening of diffraction line measured at half its maximum intensity (radians), *D* is the diameter of crystal particle, Θ is the Bragg's angle and λ is the wavelength of x-ray.

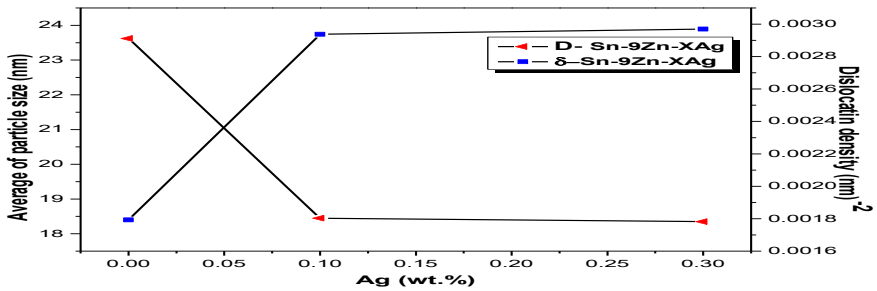

Fig (2): The particle size and dislocation density as function of Ag-additio

.

The particle size values were described in Table (1) and, compared to the β-Sn literature review, the differences between the D values may vary in the preparation method and the heat treatment method. From table (1), the particle size of β-Sn and Zn have been decreased with the Ag-additions, whereas the size of Ag3Sn increased, and the size of AgZn3 decreased with Ag-additions. The addition (0.1 and 0.3 wt.% of Ag) caused to shift only peak of Ag3Sn IMC from (303) orientation at 2θ(72.397°) to (400) orientation at 2θ (62.5°), it can see in Fig. 1(b& c), also, addition (0.1 and 0.3 wt.% of Ag) to Sn-9Zn alloys cause to shift AgZn3 IMC at 2θ (40.9˚ and 42.14˚) from (002 and 101) orientation to only (002) orientation at 2θ (40.939˚). The dislocation density (δ) calculated by using : $\delta = \frac{1}{D^2}$ - -(2) (Williamson and Hall, 1953). Its values were listed in table (1). and particle size of β-Sn as a function of Ag-addition is shown in Table (1) and Fig (2). It can be seen that there is increase in δ from (179×10^{-3} to 297×10^{-3} nm^{-2}) as more Ag added. The lattice distortions were studied and calculated according to (Williamson and Hall, 1953, Cullity, 1978): $\beta = (\frac{1}{D}) + 5 \leq \varepsilon^2 \geq^{\frac{1}{2}} Sin^{\theta}_{\lambda}$ ----**(3)**, where: *D* is the crystallite size, and (ε) is local lattice distortion in the β-Sn matrix. It is good to mention that the shifted Ag3Sn IMC and AgZn3 IMC may be caused slightly increasing lattice distortion(ε) from 1.80×10^{-3} for 0.1Ag to 1.48×10^{-3} for 0.3Ag addition to Sn-9Zn alloy (and) in the β-Sn matrix, as exhibited in table (1). A slight change has occurred in (c/a) values from (0.542) to (0.54) due to a lattice expanding in (a) and (c)-axes with Ag-additions. Also, it is noticeable that the cell volumes for all alloys have been decreased with Ag-additions as shown in table (1). The increased particle size of Ag3Sn IMC (18.5 nm) with 0.3wt.% of Ag and AgZn3 IMC (18.9 nm) with 0.1wt.% of Ag may be increased the lattice distortion (ε).

Samples in Wt.%	**D (β- Sn) (nm) In this study**	**D (β- Sn) (nm) literature review**	**D (Zn) (nm)**	**D (Ag_3Sn) (nm)**	**D ($AgZn_3$) (nm)**	**(a) Å Of (β-Sn)**	**(c) Å Of (β-Sn)**	**(c/a) Of (β-Sn)**	**V(Å)$^{-3}$ Of (β-Sn**	**(ε) x10^{-3} Of β-Sn**	**δ (nm)$^{-2}$ *10^{-3}**
Sn-9Zn	23.62	48 & 53 *	16.41	-	-	5.863	3.175	0.541	109.14	1.16	179
Sn-9Zn-0.1Ag	18.45	-	9.78	5.26	18.9	5.845	3.18	0.542	108.6	1.80	294
Sn-9Zn-0.3Ag	18.35	-	9.62	18.5	12.1	5.84	3.178	0.54	108.4	1.48	297

Table (1): The details of the XRD analysis particle size, dislocation density and lattice parameters.
* (Ismail, 2020 and (Hammam et al., 2010)**).**

3.2. Mechanical Properties

3.2.1 Creep Strain- Time

With regards to mechanical properties for the investigated materials, figures 3(a, b, c, d, e & f) showed the creep strain-time curves for Sn-9Zn and Sn-9Zn-xAg, (x = 0.0%, 0.1% and 0.3%,) alloys. The samples were investigated after annealing (T=100 ˚C) and testing at temperatures of (T= 25 ˚C, 40 ˚C, and 80 ˚C) under two different constant stresses (σ= 18.7 and 24.94 MPa). From figs. 3(a, c and e), its presented that the creep time and resistance of Sn-9Zn- 0.3 Ag alloy with 18.7 MPa load are the longest compared to that of the eutectic Sn-9Zn and Sn-9Zn-0.1 Ag alloys. And from figs.3(b, d and f), the creep time and resistance of Sn-9Zn-0.1 Ag alloy with 24.94 MPa load are the longest compared to the eutectic Sn-9Zn and Sn-9Zn-0.3 Ag alloys. In general, the creep resistance of Sn-9Zn-xAg 0.1 and 0.3Ag alloys was higher than of Sn-9Zn alloy, may be due to the refinement of structure and IMCs formation, and these mechanical improvements are attributed to the high structural stability of Sn-9Zn-0.1 and 0.3Ag alloys compared to the Sn-9Zn. The formations of Ag3Sn and AgZn3 IMCs in the ternary alloys can result in impeding the dislocation movement more efficiently, and produce an alloy with lower creep rate. Similar phenomena that agree with Mahmudi et al, (Mahmudi et al., 2009) can be found for Sn–9Zn alloy with addition of Ag. The creep strain rate (S^{-1}) of the Sn-9Zn-XAg alloys was calculated by using the slope between Strain-Time Curves in the secondary stage as shown in Figures3 (a to f). Figs. 3(c, e and f) for three Alloys showed the third Stage of creep, while from Figs. 3(a, b and e) the behavior of creep for three Alloys were showed only in two creep stages. From Table(2) and fig(4), with added amount of Ag to Sn-9Zn, the secondary creep rate (strain rate $(\dot{\varepsilon})$ decreases while the creep life increases at this stage at different temperatures and loads . It's may be due to its large lattice distortion. Although the enhanced rupture time and creep rate(S^{-1}) of the Sn-9Zn alloys with Ag additions, also the reason is may be due to an appearance of IMCs (AgZn3(Hex) and Ag_3Sn (Orthorhombic) phases), with Ag-additions to Sn-9Zn Alloys which is basically returned to their different crystal structures (Zhao et al., 2019).

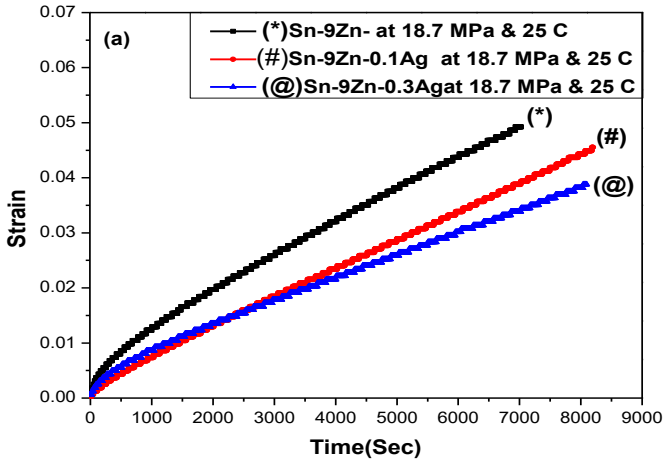
(a)
(*)Sn-9Zn- at 18.7 MPa & 25 C
(#)Sn-9Zn-0.1Ag at 18.7 MPa & 25 C
(@)Sn-9Zn-0.3Agat 18.7 MPa & 25 C
Strain
Time(Sec)

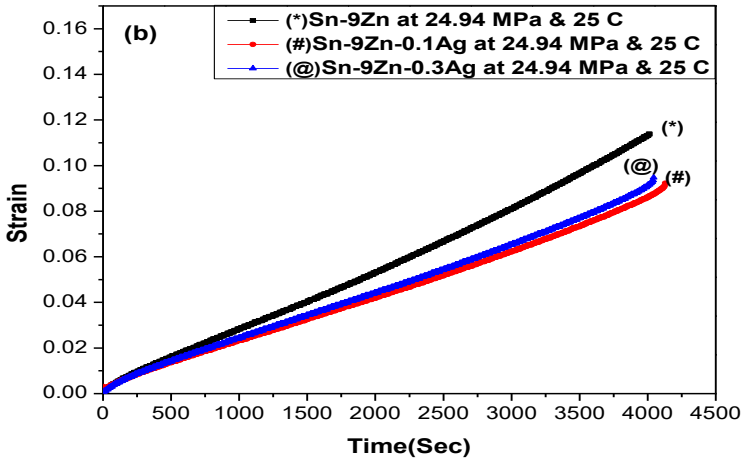
(b)
(*)Sn-9Zn at 24.94 MPa & 25 C
(#)Sn-9Zn-0.1Ag at 24.94 MPa & 25 C
(@)Sn-9Zn-0.3Ag at 24.94 MPa & 25 C
Strain
Time(Sec)

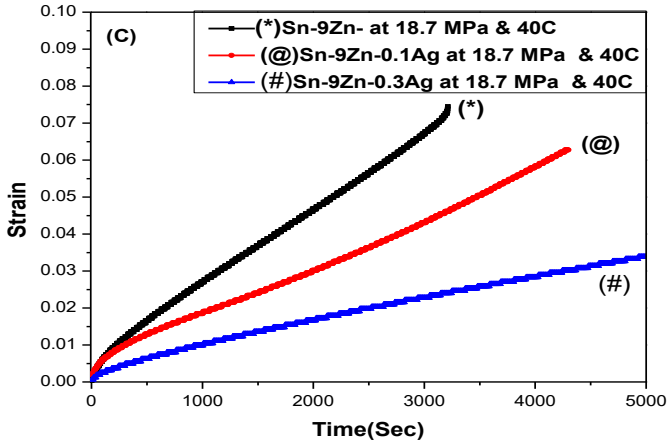
(C)
(*)Sn-9Zn- at 18.7 MPa & 40C
(@)Sn-9Zn-0.1Ag at 18.7 MPa & 40C
(#)Sn-9Zn-0.3Ag at 18.7 MPa & 40C
Strain
Time(Sec)

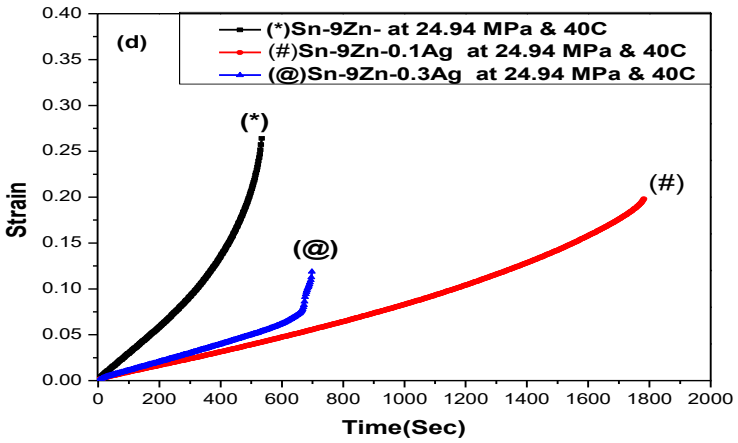
(d)
(*)Sn-9Zn- at 24.94 MPa & 40C
(#)Sn-9Zn-0.1Ag at 24.94 MPa & 40C
(@)Sn-9Zn-0.3Ag at 24.94 MPa & 40C
Strain
Time(Sec)

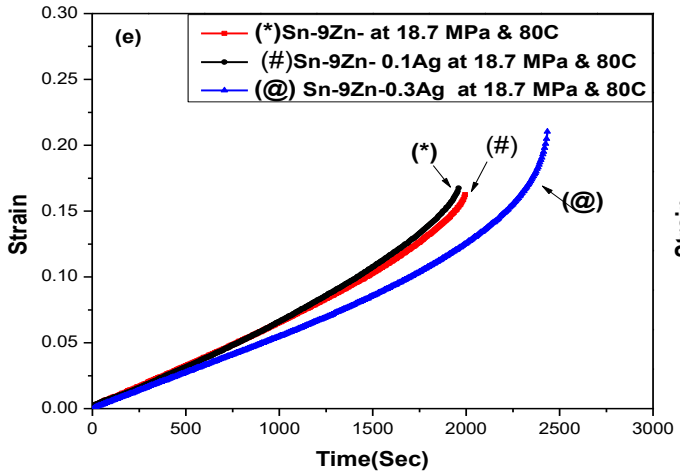
(e)
(*)Sn-9Zn- at 18.7 MPa & 80C
(#)Sn-9Zn- 0.1Ag at 18.7 MPa & 80C
(@) Sn-9Zn-0.3Ag at 18.7 MPa & 80C
Strain
Time(Sec)

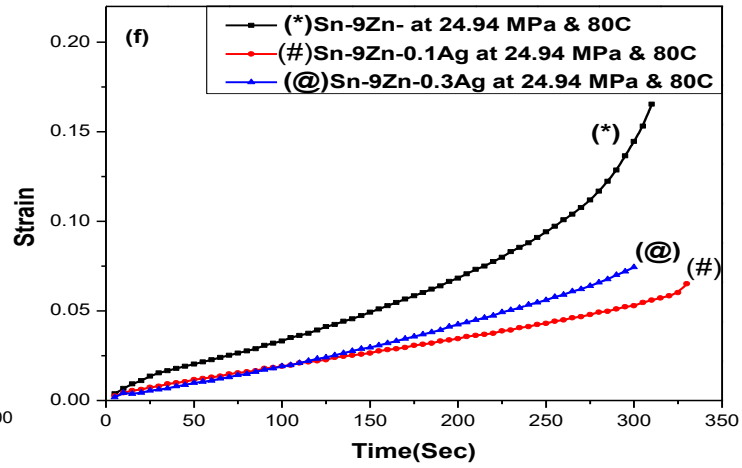
(f)
(*)Sn-9Zn- at 24.94 MPa & 80C
(#)Sn-9Zn-0.1Ag at 24.94 MPa & 80C
(@)Sn-9Zn-0.3Ag at 24.94 MPa & 80C
Strain
Time(Sec)

Samples in Wt.%	Creep rate(S^{-1}) at 18.7 MPa			Creep rate(S^{-1}) at 24.94 MPa		
Tem.	25 ˚C	40 ˚C	80 ˚C	25 ˚C	40 ˚C	80 ˚C
Sn-9Zn	5.17E-6	1.98E-5	7.57E-5	2.92E-5	1.37E-4	3E-4
Sn-9nZ-0.1Ag	5.18E-6	1.28E-5	6.57E-5	1.98E-5	8.72E-5	1.56E-4
Sn-9nZ-0.3Ag	4.16E-6	1.42E-5	6.1E-5	2E-5	9.73E-5	2.2E-4

Figs. (3) Creep strain-time curves for Sn-9Zn-XAg at **a**) T=25 ˚C &18.7 MPa, **b**) T=25 ˚C & 24.94MPa, **C**) T=40 ˚C &18.7 MPa, **d**) T=40 ˚C &24.94 MPa, **e**) T=80˚ C &18.7 MPa and **f**) T=80 ˚C&18.7 MPa.

Table (2): The variation of creep rate of three samples with Ag-addition.

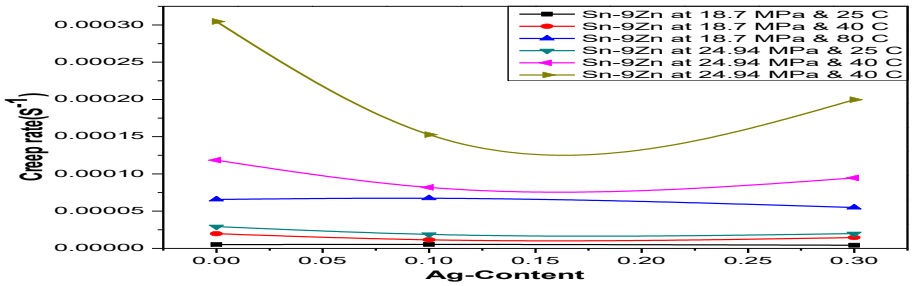

Fig. (4) The creep rate ($\dot{\varepsilon}$) for Sn-9Zn-XAg at T= 25 ˚C, 40˚and 80 ˚C under 18.7 and 24.94 MPa.

The Elongation (El.%) was calculated for all the figures 3(a to f), by using equation: **(EL.%= Strain × 100) --- (4)**. The El.% plots are drawn in Fig (5), and its values were listed in the Table (3) for three alloys.

Samples in Wt.%	EL.%					
	18.7 MPa			24.94 MPa		
Tem.	25 ˚C	40 ˚C	80 ˚C	25 ˚C	40 ˚C	80 ˚C
Sn-9Zn	4.92325	7.44558	16..73592	11.38183	26.39442	16.54792
Sn-9Zn-0.1Ag	4.55117	6.2745	16.24242	9.22767	19.8105	6.52125
Sn-9Zn-0.3Ag	3.8775	6.64267	21.04033	9.47442	11.87533	7.44558

Table (3): The variation of elongation of three samples with Ag-addition.

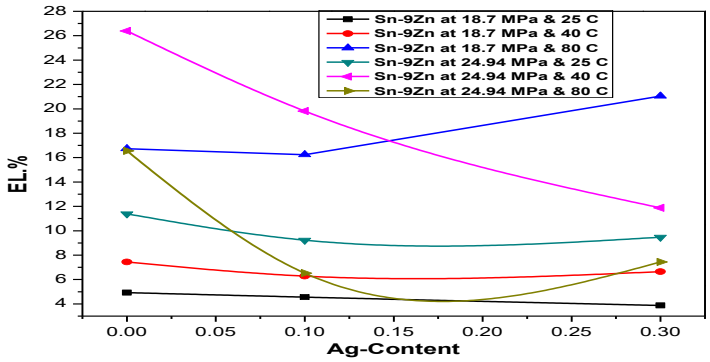

Fig. (5). The El. (%) for Sn-9Zn-XAg at (T= 25 ˚C, 40˚and 80 ˚C) under 18.7 and 24.94 MPa.

The Elongation of Sn-9Zn- 0.3 Ag alloy at T=80˚ C with 18.7 MPa load is the longest compared to that of the eutectic Sn-9Zn and Sn-9Zn-0.1 Ag alloys as shown in Fig.(3e). The EL.% of Sn-9Zn at T= 25℃, 40℃ and 80℃ under 18.7 and 24.94 MPa are increasing compared to The EL.% of Sn-9Zn -0.1Ag at the same load as shown in figs. 3(a, b, c, d and f). These results may be represent the dissolution of Zn or AgZn3 IMCs (Ismail, 2020).

3.2.1.1 Creep stress exponents and activation energy for Sn-9Zn-XAg Alloys

The stress exponent (n) parameter and activation energy(Q) of steady state creep were calculated by using equations: (Rahman et al., 2009): **($n = \frac{\partial Ln(\dot{\varepsilon})}{\partial Ln(\sigma)}$) ---- (5)** and **$Q = -R\left(\frac{\partial Ln(\dot{\varepsilon})}{\partial Ln\left(\frac{1}{T}\right)}\right)$ ---- (6)**, the calculated values of n and Q at different temperatures and loads for the tested alloys are listed in the Table (4) and, compared to the Sn-9Zn-xAg Alloy literature review, the differences between n and Q values may vary in the preparation method and the heat treatment method. The results of the values of stress exponents, as shown in Fig. (6)and given in Table (4) that compared with literature review for Sn-9Zn alloy, its decrease from n= (6 to 4.64 and 5.52) at T= 25℃, n= (4 to 2.51 and 4.4) at T= 40℃ and n= (6.7 to 6.65 and 6.68) at T= 80℃ for Sn-9Zn, Sn-9Zn-0.1Ag and Sn-9Zn-0.3Ag respectively. The difference between n values for all alloys at different temperatures is due to the dislocation movement (climb-creep) mechanism, as documented by (Kanda and Kariya, 2012, Wiese et al., 2008). While, at temperature (T= 80 ˚C) the n value of Sn-9Zn-0.1Ag alloy is due to the dislocation movement (slip-creep) mechanism

.

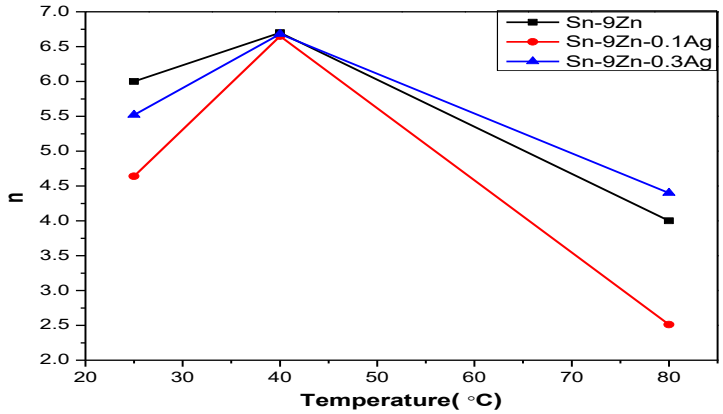

Fig. (6): The stress exponent(n) values at different temperature with Ag-addition.

Also, the activation energies in steady state creep of three alloys were calculated from the slope of relation between Ln (Creep rate) and 1000/T at (T=25 ˚C, 40 ˚C and 80 ˚C) in the Figs. 7(a and b), with two different applied stresses. It is noticeable that Q decreases with the increase of applied stress that depends strongly on applied stress and temperatures (Wu and Huang, 2002). The Q increases with increasing Ag addition to Sn-9Zn alloy. It was observed that Sn-9Zn -0.1 and 0.3Ag has the highest Q values depending on creep resistance, as documented by (Mahmudi et al., 2009, Khalifa et al., 2017, El-Daly and Hammad, 2010).

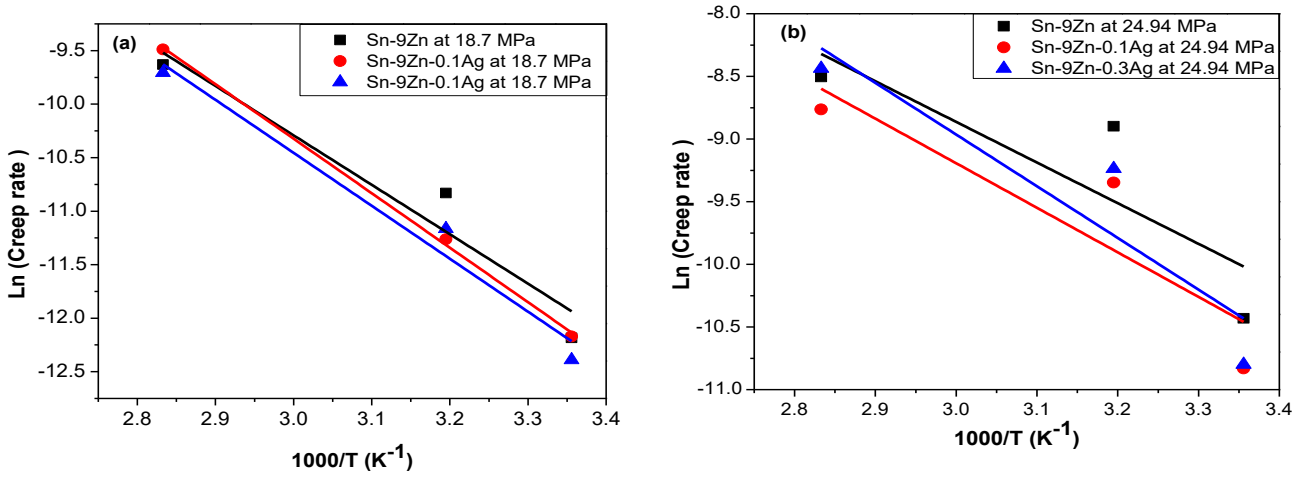

Fig. (7) The relation between Ln($\dot{\varepsilon}$) and 1000/T for Sn-9Zn-XAg Alloys at a)18.7 MPa and b) 24.94 MPa.

.

Alloys	Q(KJ/mol) 18.7 MPa	Q(KJ/mol) 24.94 MPa	Temperature (°C)	(n) This study	(n) literature review	Q(kJ/mol) literature review
Sn-9Zn	36.48	27	25	6	7 & 5 (El-Daly et al., 2014 & Shrestha et al., 2014)	42.1[a]
			40	6.7		
			80	4		
Sn-9Zn-0.1Ag	41.14	30	25	4.64	7.1[a]	42.9[a]
			40	6.65		
			80	2.51		
Sn-9Zn-0.1Ag	42.32	34.3	25	5.52		
			40	6.68		
			80	4.4		

Table (4): Activation energy (Q) and stress exponent (n) values for Sn–9Zn, Sn–9Zn–0.1Ag and Sn–9Zn–0.3Ag solder alloys [a](Sn-9Zn-0.5Ag at load 60 to130 MPa and at T= 298 K to 370 K (Mahmudi et al., 2009b)).

3.3. Electrical resistivity and conductivity

With respect to electrical properties, electrical resistivity(ρ) and conductivity(σ) were calculated by using equations:

$\rho = R\frac{A}{l}$ --- **(7)** and $\sigma = \frac{1}{\rho}$ ---- **(8),** receptively,

Where L is length of the specimen, R is the ohm resistance and A is the cross-section area (Callister, 2007, La Barre, 2004). The electrical resistivity and conductivity of Sn-9Zn-XAg alloys at room temperature (T= 25 °C) are shown in Table (5) and Fig. 8(a & b), in general the ρ values have decreased with Ag additions, but the σ values have increased with Ag additions. This decrease and increase for ρ and σ are may be due to enhancing the Ag3Sn and AgZn3 formation in Sn-9Zn Alloys with Ag-Additions.

Samples in Wt.%	ρ (Ω-Cm) * 10^{-3}	σ $(\Omega\text{-Cm})^{-1}$
Sn-9Zn	**1.83**	**546.45**
Sn-9Zn-0.1Ag	**1.13**	**884.96**
Sn-9Zn-0.3Ag	**1.12**	**892.88**

Table (5): The variation of (ρ) and (σ) for three samples with Ag-addition at room temperature (T= 25 °C).

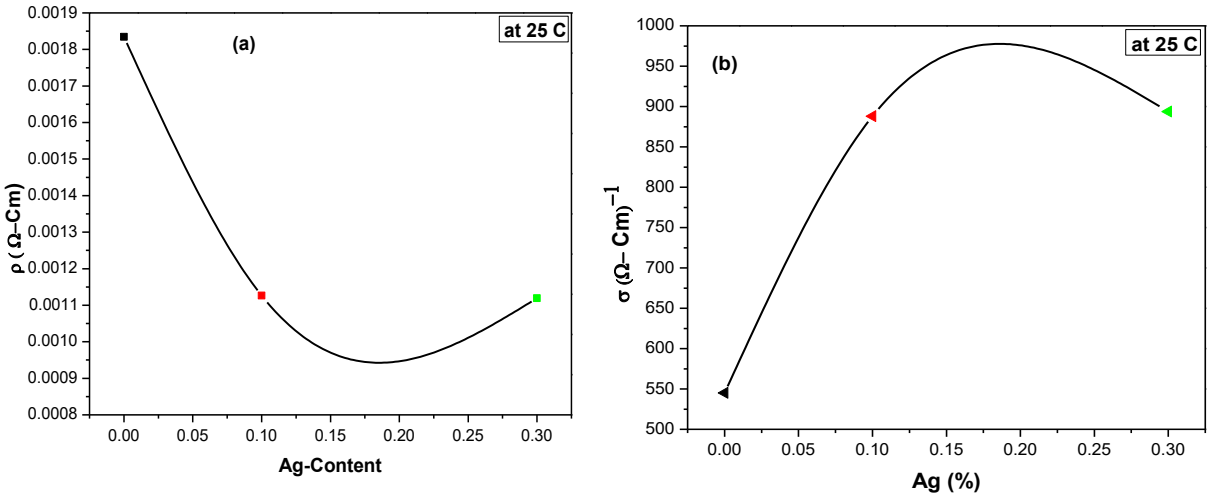

Fig. (8): **a)** Electrical resistivity behaviour for Sn-9Zn alloys with Ag additions at T= 25 °C and **b)** Electrical conductivity behaviour for Sn-9Zn alloys with Ag additions at T= 25 °C.

4. Conclusions

This study has investigated the Silver(Ag) improvements in two concentrations (0.1 and 0.3 wt.%) on the structural, Mechanical (Creep resistance) and electrical conductivity properties of eutectic Sn-9Zn alloy. The results are summarized as follows: With the addition of Ag to Sn-9Zn eutectic alloys leads to the formation of body cantered tetragonal β-Sn, hexagonal Zn, Orthorhombic Ag3Sn and Hexagonal AgZn3 phases. The average particle size (D) of β-Sn phases decreased continuously with addition of (0.1 and 0.3 wt.% Ag), while The dislocation density (δ) increased with Ag-additions. The creep resistance of Sn-9Zn-0.1Ag and Sn-9Zn-0.3Ag Alloys are higher than that of Sn-9Zn alloys at different temperature and loads due to the refinement structure and formation of new IMCs. The n values are due to that the deformation mechanism is the dislocation climb for all alloys at different temperatures. Except at T= 80 ˚C for Sn-9Sn-0.1Ag alloy, the dislocation movement (slip-creep) is controlling mechanism. In general, increasing of Q with (0, 0.1 and 0.3 Ag)-addition to Sn-9Zn Alloys depends on creep resistance. Also, the decrease of Q with the increase of applied stress depends strongly on applied stress and temperature. The decrease and increase for ρ and σ are may be due to enhancing the Ag3Sn and AgZn3 formation in Sn-9Zn Alloys with Ag- additions.

Reference

[1]. AHMED, M., FOUZDER, T., SHARIF, A., GAIN, A. K. & CHAN, Y. C. (2010). Influence of Ag micro-particle additions on the microstructure, hardness and tensile properties of Sn–9Zn binary eutectic solder alloy. *Microelectronics Reliability,* 50**,** 1134-1141.

[2]. CALLISTER, W. D. (2007). *Materials science and engineering an introduction*, John Wiley.

[3]. CHEN, W., XUE, S., WANG, H., WANG, J. & HAN, Z. (2009). Solderability and intermetallic compounds formation of Sn-9Zn-xAg lead-free solders wetted on Cu substrate. *Rare Metals,* .656 ،28

[4]. CHENG, S., HUANG, C.-M. & PECHT, M. (2017). A review of lead-free solders for electronics applications. *Microelectronics Reliability,* 75**,** 77-95.

[5]. CULLITY, B. (1978). Elements of X-ray Diffraction. Addison and Wesley Publishing Company Inc. *Reading, USA***,** 32-106.

[6]. EL-DALY, A., DESOKY, W., SAAD, A., MANSOR, N., LOTFY, E., ABD-ELMONIEM, H. & HASHEM, H. (2015). The effect of undercooling on the microstructure and tensile properties of hypoeutectic Sn–6.5 Zn–xCu Pb-free solders. *Materials & Design,* 80**,** 152-162.

[7]. EL-DALY, A. & HAMMAD, A. (2010). Effects of small addition of Ag and/or Cu on the microstructure and properties of Sn–9Zn lead-free solders. *Materials Science and Engineering: A,* 527**,** 5212-5219.

[8]. EL-DALY, A., HAMMAD, A., AL-GANAINY, G. & IBRAHIEM, A. (2014). Design of lead-free candidate alloys for low-temperature soldering applications based on the hypoeutectic Sn–6.5 Zn alloy. *Materials & Design (1980-2015),* 56**,** 594-603.

[9]. GAIN, A. K. & ZHANG, L. (2016). Harsh service environment effects on the microstructure and mechanical properties of Sn–Ag–Cu-1 wt% nano-Al solder alloy. *Journal of Materials Science: Materials in Electronics,* 27**,** 11273-11283.

[10]. GAIN, A. K. & ZHANG, L. (2020). Nanoindentation Creep, Elastic Properties, and Shear Strength Correlated with the Structure of Sn-9Zn-0.5 nano-Ag Alloy for Advanced Green Electronics. *Metals,* 10**,** 1137.

[11]. GARCIA, L. R., OSORIO, W. R., PEIXOTO, L. C. & GARCIA, A. (2010). Mechanical properties of Sn–Zn lead-free solder alloys based on the microstructure array. *Materials Characterization*, 61**,** 212-220.
[12]. GUODA, E., MAHASI, A., HADADI, K. & FAQEEH, A. (2014). Study the structure and electrical properties of Sn-9Zn-1Ag solder alloy. *International Journal of Physics and Astronomy*, 2**,** 123-128.
[13]. HAMADA, N., HAMADA, M., UESUGI, T., TAKIGAWA ،Y. & HIGASHI, K. (2010). Effect of small addition of zinc on creep behavior of tin. *Materials transactions***,** 1009131184-1009131184.
[14]. HAMMAM, M., ALLAH, F. S., GOUDA, E. S., EL GENDY, Y. & AZIZ, H. A. (2010). Structure and properties of Sn-9Zn Lead-free solder alloy with heat treatment. *Engineering*, 2**,** 172-178.
[15]. ISMAIL, R. A. (2020). Investigation of Microstructure and Mechanical Properties of Different Nano-Particles Doped Sn-Zn Lead-Free Solder Alloys. *Arab Journal of Nuclear Sciences and Applications*, 53**,** 191-.199
[16]. KANDA, Y. & KARIYA, Y. (2012). Evaluation of creep properties for Sn–Ag–Cu micro solder joint by multi-temperature stress relaxation test. *Microelectronics Reliability*, 52**,** 1435-1440.
[17]. KHALIFA, B., ISMAIL, R. A. & YASSIN, A. (2017). Structure Analysis, Enhancement of Creep Resistance and Thermal Properties of Eutectic Sn-Ag Lead-Free Solder Alloy by Ti and Cd Additions. *Journal of Advances Physics*, 1**,** 5092-5099.
[18]. KNOTT, S. & MIKULA, A. (2002). Thermodynamic properties of liquid Al-Sn-Zn alloys: A possible new lead-free solder material. *Materials transactions*, 43**,** 1868-1872.
[19]. KOTADIA, H. R., HOWES, P. D. & MANNAN, S. H. (2014). A review: On the development of low melting temperature Pb-free solders. *Microelectronics Reliability*, 54**,** 1253-1273.
[20]. LA BARRE, K. A. (2004) .The Art and Science of Classification: Phyllis Allen Richmond, 1921—1997.
[21]. LIU, C.-Y., HON, M.-H., WANG, M.-C., CHEN, Y.-R., CHANG, K.-M. & LI, W.-L. (2014). Effects of aging time on the mechanical properties of Sn–9Zn–1.5 Ag–xBi lead-free solder alloys. *Journal of alloys and compounds*, 582**,** 229-235.
[22]. MAHMUDI, R., GERANMAYEH, A., NOORI, H. & TAGHADDOSI, M. (2009). Effects of Ag and Al additions on the structure and creep properties of Sn-9Zn solder alloy. *Journal of electronic materials*, 38**,** 330-337.
[23]. PENG, F., LIU, W., MA, Y., LIANG, C., HUANG, Y. & TANG, S. (2019). Microstructure of Sn-20In-2.8 Ag solder and mechanical properties of joint with Cu. *Soldering & Surface Mount Technology*.
[24]. RAHMAN, M., SHARIF, A. & AHMED, M. (2009). Effect of various amount of Cu on the thermal and mechanical behavior of Sn-9Zn eutectic Pb-free solder alloy. Proceedings of the International Conference on Mechanical Engineering (ICME2009),. 26-28.
[25]. SALEM, D. (2020). Influence of Cu Addition on the Transient Creep Characteristics of Sn–9Zn-1.5Ag Solder Alloy. *American Research Journal of Physics*, 6**,** 1-11.
[26]. SHRESTHA, T., GOLLAPUDI, S., CHARIT, I. & MURTY, K. L. (2014). Creep deformation behavior of Sn–Zn solder alloys. *Journal of Materials Science*, 49**,** 2127-2135.
[27]. VUONG, B., VU, N., MANH ،T., VAKA, M., DU, D. & NAM, N. (2018). Role of cerium in microstructure and corrosion properties of Sn-1.0 Ag solder alloys. *Materials Letters*, 228**,** 309-313.
[28]. WIESE, S., ROELLIG, M., MUELLER, M. & WOLTER, K.-J. (2008). The effect of downscaling the dimensions of solder interconnects on

their creep properties. *Microelectronics Reliability*, 48**,** 843-850.
[29]. WILLIAMSON, G. & HALL, W. (1953). X-ray line broadening from filed aluminium and wolfram. *Acta metallurgica*, 1**,** 22-31.
[30]. WU, C. L. & HUANG, M. (2002). Creep behavior of eutectic Sn-Cu lead-free solder alloy. *Journal of electronic materials*, 31**,** 442-448.
[31]. XU, K.-K., ZHANG, L., GAO, L.-L., JIANG, N., ZHANG, L. & ZHONG, S.-J. (2020). Review of microstructure and properties of low temperature lead-free solder in electronic packaging. *Science and Technology of Advanced Materials*, 21**,** 689-711.
[32]. ZHANG, L. & TU, K.-N. (2014). Structure and properties of lead-free solders bearing micro and nano particles. *Materials Science and Engineering: R: Reports*, 82**,** 1-32.
[33]. ZHAO, M., ZHANG, L., LIU, Z.-Q., XIONG, M.-Y. & SUN, L. (2019). Structure and properties of Sn-Cu lead-free solders in electronics packaging. *Science and technology of advanced materials*, 20**,** 421-444.
[34]. ZHU, W., ZHANG, W., ZHOU, W. & WU, P. (2019). Improved microstructure and mechanical properties for SnBi solder alloy by addition of Cr powders. *Journal of Alloys and Compounds*, 789**,** 805-813.